NUMERICAL STUDY OF SHALLOW WATER WAVE SPECTRUM

[1]SHUOYANG WANG

SUPERVISOR: [1]DMITRY E. PELINOVSKY

Abstract. In this work, we studied the spectrum of a local linearized linear operator for the shallow water wave, which is reduced from the conformal Euler's equations for Stokes' wave [2]. We report the numerical instability for the smooth wave $\eta \in C^\infty_{\rm per}(\mathbb{T})$ in the limit of the singular peaked wave $\eta \in C^0_{\rm per}(\mathbb{T}) \cap W^{1,\infty}(\mathbb{T})$, and this indicates the peaked wave cannot be considered as the sequential limit of smooth waves.

1. Introduction

The Stokes' wave is proposed by Sir George Stokes in 19th century [1, 6], and it has been studied from different perspectives over last 150 years [3, 4, 5]. In this work, Euler's equations with two canonical variables in the holomorphic coordinate are used to describe the Stokes' wave [7], and this model is further reduced to a local version in shallow water limit [2].

For the reduction of model, consider the incompressible and irrotational 2D fluid described by the Euler's equations. The solutions are 2π-periodic travelling wave $\eta(x,t)$ with single crest in the periodic region $(x,y) \in [-\pi,\pi] \times [-h_0, \eta(x,t)]$. They have zero vertical velocity at the flat bottom $\eta = -h_0$ and zero-mean constraint on the surface. The conformal transformation $x + iy \mapsto z(u+iv,t)$ is applied to obtain the solution $\eta(u,t)$ in the holomorphic coordinate, where $\mathbb{T} = \mathbb{R}\backslash(2\pi\mathbb{Z})$ denotes the corresponding 2π-periodic domain, and the region changes to be a rectangular region $(u,v) \in [-\pi,\pi] \times [-h,0]$ with flat surface at $v = 0$ and flat bottom at $v = -h$. The further reduction from the non-local model to the local model is achieved by removing the local term $1/h$ in the nonlocal operator, and this gives the nonlinear PDE

$$2c\frac{\partial}{\partial u}\left(\frac{\partial \eta}{\partial t}\right) = (c^2 - 2\eta)\frac{\partial^2 \eta}{\partial u^2} - \left(\frac{\partial \eta}{\partial u}\right)^2 + \eta, \tag{1}$$

where $c > 0$ is the wave speed, and the existence of the solution requires $\eta(u)$ to satisfy the ODE

$$(c^2 - 2\eta)\eta'' - (\eta')^2 + \eta = 0. \tag{2}$$

This reduced model was studied in [2]. As the preliminary information, the following theorems are stated without proofs, and the detailed formalisms can be found in [2]. Theorem 1 addresses the existence of solution for the local model.

Definition 1. The solution profile $\eta(u)$ is single-lobe if there exists a single maximum and minimum on $\mathbb{T}$.

Theorem 1 (Theorem 1, [2])**.** *There exist $c_* = \frac{\pi}{2\sqrt{2}}$ and $c_\infty \in (c_*, +\infty)$ for the ODE (2), which has a single-lobe unique solution $\eta \in C^\infty_{\rm per}(\mathbb{T})$ for every $(1, c_*)$ such that*

$$\lim_{c \to 1} \|\eta\|_{L^\infty} = 0. \tag{3}$$

and a single lobe solution $\eta \in C^0_{\rm per}(\mathbb{T})$ for every $c \in (c_*, c_\infty)$ satisfying

$$\eta(u) = \frac{1}{2}c^2 - A(c)|u|^{2/3} + \mathcal{O}(u) \tag{4}$$

as $u \to 0$ for some constant $A(c) > 0$. For $c = c_*$, there exists a unique even solution with the profile $\eta \in C^0_{\rm per}(\mathbb{T}) \cap W^{1,\infty}(\mathbb{T})$ given explicitly as

$$\eta|_{c^*}(u) = \frac{1}{16}(\pi^2 - 4\pi|u| + 2u^2), \quad u \in \mathbb{T}. \tag{5}$$

Date: July 9, 2024.

[1]Department of Mathematics and Statistics, McMaster University, Hamilton, Ontario, L8S 4L8.

After taking the zero-mean constraint and integration by parts, the linear stability problem can be formulated by considering the perturbation $\gamma = \gamma(u,t), t > 0$ respect to the solution $\eta(u)$, such that

$$2c\frac{\partial \gamma}{\partial t} = -\Pi_0 \partial_u^{-1} \Pi_0 \mathcal{L}\gamma., \qquad \mathcal{L} = -\frac{\partial}{\partial u}(c^2 - 2\eta)\frac{\partial}{\partial u} + (2\eta'' - 1), \tag{6}$$

where the projection operator $\Pi_0 : L^2(\mathbb{T}) \to L^2(\mathbb{T})|_{\{1\}^T}$ determines the antiderivative uniquely by requiring zero-mean constraint over the periodic domain $\mathbb{T}$, and the local linear operator is denoted as $\mathcal{L}$. Theorem 2 characterizes the eigenvalue properties of this local linear operator.

Theorem 2 (Lemma 5, [2]). *Let $\eta \in C^\infty_{\text{per}}(\mathbb{T})$ be the smooth solution in $c \in (1, c_*)$, and $\mathcal{L} : H^2_{\text{per}}(\mathbb{T}) \subset L^2(\mathbb{T}) \to L^2(\mathbb{T})$ be the linear operator in (6). There are two simple negative eigenvalues $\lambda_1, \lambda_2 < 0$ and a simple zero eigenvalue $\lambda_3 = 0$, and the rest of eigenvalues are all positive ($\lambda_i > 0, i > 3$).*

Remark 1. We refer $\eta \in C^\infty_{\text{per}}(\mathbb{T})$ with $c \in (1, c_*)$, $\eta \in C^0_{\text{per}}(\mathbb{T}) \cap W^{1,\infty}(\mathbb{T})$ at $c = c_*$ and $\eta \in C^0_{\text{per}}(\mathbb{T})$ with $c \in (c_*, c_\infty)$, as the smooth, peaked, and cusped waves, respectively. Without loss of generality, the spectrum is studied in the smooth wave region, and the numerical computations are done for first five eigenvalues $\lambda_1, \ldots, \lambda_5$.

Equation (1) is known as one version of Hunter-Saxton's equation, which was first studied by Hunter and Saxton in 1991 [8, 10]. This model is commonly used to study the non-linear instability in the directional field of a nematic liquid crystal, and it is also shown as the high frequency limit of another water wave model Camassa-Holm equation [9], which has the similar peaked solution (5) with the finite jump of first derivative at crest [11].

In this work, we emphasize the numerical methods to examine the spectrum of this local linear operator $\mathcal{L}$. The solution profiles $\eta(u)$ are approximated in Section 2, and the finite difference method and Fourier collocation method are developed in Section 3 to study the spectrum of the operator $\mathcal{L}$.

2. Approximation of Travelling Wave Profile

In this section, we discuss the numerical approximation of solution η to (2). Since the Fourier collocation method is used in Section 3, we will examine the solution profiles in both physical and Fourier space in this section.

Firstly, we consider the solutions in physical space. By theorem 1, the existence of the solution for the local model requires $\eta(u)$ to satisfy the ODE model (2), which has its first invariant written as the level sets

$$\mathcal{E}(c) = \frac{1}{2}\left[(c^2 - 2\eta)(\eta')^2 + \eta^2\right]. \tag{7}$$

This equation can be used to solve for $\eta(u)$ implicitly with respect to the C^1 boundary conditions at $u = \pm\pi$ in the holomorphic periodic domain $u \in [-\pi, \pi]$, such that

$$\begin{cases} \left(\dfrac{d\eta}{du}\right)^2 = \dfrac{2\mathcal{E} - \eta^2}{c^2 - 2\eta} \\ \eta(\pm\pi) = -\sqrt{2\mathcal{E}}, \quad \eta'(\pm\pi) = 0 \end{cases}, \tag{8}$$

and the solution profile $\eta(u)$ can be obtained by finding the root of the integral equation

$$f(\eta) - u = 0, \qquad f(\eta) = \begin{cases} \displaystyle\int_{\eta/\sqrt{2\mathcal{E}}}^{1} \frac{\sqrt{c^2 - 2\sqrt{2\mathcal{E}}x}}{\sqrt{1-x^2}}\,dx & \mathcal{E} \le \mathcal{E}_* \\ \displaystyle\int_{\eta/\sqrt{2\mathcal{E}}}^{c^2/2\sqrt{2\mathcal{E}}} \frac{\sqrt{c^2 - 2\sqrt{2\mathcal{E}}x}}{\sqrt{1-x^2}}\,dx & \mathcal{E} > \mathcal{E}_* \end{cases}, \tag{9}$$

where $\mathcal{E}_* := \mathcal{E}(c_*) = c^4/8$. Since the solutions are in even parity, for convenience, we only consider half of the domain $[0, \pi]$, where even reflection gives the full solution profile, and this allows us to take only negative sign from (8) for the function $f(\eta)$ in (9). To determine the parameters $(\mathcal{E}(c), c)$ in $c \in (1, c_\infty)$, consider the

period functions $T(\mathcal{E}, c)$, which can be represented using the complete elliptic integrals of first and second kind $K(\kappa), E(\kappa)$ with eccentricity $\kappa > 0$, such that

$$T(\mathcal{E},c) = \begin{cases} 4E(\kappa)\sqrt{c^2+2\sqrt{2\mathcal{E}}} & (\mathcal{E},c) \in (0,\mathcal{E}_*)\times(1,c_*) \\ 4(2\mathcal{E})^{1/4}\left[2E(\kappa)+\left(\dfrac{c^2}{2\sqrt{2\mathcal{E}}}-1\right)K(\kappa)\right] & (\mathcal{E},c)\in(\mathcal{E}_*,\mathcal{E}_\infty)\times(c_*,c_\infty) \end{cases}, \ \kappa = \sqrt{\frac{4\sqrt{2\mathcal{E}}}{c^2+2\sqrt{2\mathcal{E}}}}, \tag{10}$$

and this allows us to determine each parameter pair $(\mathcal{E}, c)$ uniquely by setting the constraint $T(\mathcal{E}, c) = 2\pi$. Note that the parameters at the critical value of the peaked wave is $\mathcal{E}_* = c^4/8$, and the limiting case of cusped waves are $\mathcal{E}_\infty := \mathcal{E}(c_\infty)$, which cannot determined analytically. To approximate the solution profile numerically, let $u_j = jh, j \in \{0, \dots, N\}, N \in \mathbb{Z}^+$ be a fixed grid with the step size $h = \pi/N$. By the fundamental theorem of calculus, the solution profile $\{(\eta_j, u_j)\}_{j=0}^N$ can be found by solving $f(\eta_j) - u_j = 0$ for every j. Implement the Newton–Raphson's method as the root-finding algorithm under a specific tolerance $\epsilon > 0$, such that

$$\eta_j^{(k+1)} = \eta_j^{(k)} - \frac{1}{f'\left(\eta_j^{(k)}\right)}\left[f\left(\eta_j^{(k)}\right) - u_j\right], \qquad \left|f\left(\eta_j^{(k)}\right) - u_j\right| \le \epsilon, \tag{11}$$

where k denotes iteration number and we take $\eta_0(0) = \sqrt{2\mathcal{E}}$ and $\eta_N(\pi) = -\sqrt{2\mathcal{E}}$ as two boundary grid points to avoid the weak singularities. Given a c-grid $\{c_i\}_{i=1}^M$ with $M \in \mathbb{Z}^+$ grid points, the period function (10) computes $\mathcal{E}_i$ respect to c_i, which is closest to the input c value. This output the the sets of parameter pairs $\{(\mathcal{E}_i, c_i)\}_{i=1}^M$, which can be used in the root-finding algorithm (11), and it allows us to determine the critical value $c_\infty \in (c_*, +\infty)$ and the corresponding $\mathcal{E}_\infty \in (\mathcal{E}_*, +\infty)$ from the 2π constraint numerically. After the solutions $\{(\eta_j, u_j)\}_{j=0}^N$ are obtained on $[0, \pi]$ for $N + 1$ grid points, the even reflection fills all $2N + 1$ grid points on $[-\pi, \pi]$ domain, and the solution profiles in physical space are plotted in Figure 1.

Next, we consider the solution in Fourier space. Since the solutions in physical space η are discretized, the solutions in Fourier space $\hat{\eta}$ can be found using the discrete Fourier transform (DFT) with $2N+1$ modes in Fourier space, such that

$$\hat{\eta}_n = \frac{h}{2\pi}\sum_{j=-N}^{N-1}\eta_j e^{-inu_j}, \qquad n \in \{-N, \dots, N\} \tag{12}$$

where one of the end point $u_N = \pi$ in physical space is removed because of the 2π-periodicity. For the limiting peaked wave (5) at $c = c_*$, it can be represented as Fourier cosine series, such that

$$\eta|_{c^*}(u) = -\frac{\pi^2}{48} + \sum_{m=1}^{\infty}\frac{\cos(mu)}{2m^2}. \tag{13}$$

By applying DFT on the selected grid, solution profiles in Fourier space can be plotted for both smooth and singular waves.

Remark 2. The Figure 1 elucidates the properties of solution profiles in both physical and Fourier space for smooth, peaked, and cusped waves. Here we remark some key features in the figure.

- The solution profiles in physical space agree with theorem 1: the smooth solutions η are differentiable; the peaked solution has a first derivative with finite jump discontinuity ($\eta' \in L^\infty(\mathbb{T})$); and the cusped solutions have first derivatives with a vertical asymptote ($\eta' \notin L^\infty(\mathbb{T})$).
- The amplitude of smooth waves approaches zero as the limit (3), and the cusped waves attain the maximum amplitude at c_∞, which is the bifurcation point and the singular solution on the other branch is not considered here.
- In Fourier space, the smooth waves do not converge well to zero as approaching to the peaked waves ($c \to c_*^-$), and this explains the numerical crush of the Fourier collocation method in Section 3, indicating that it is not valid to consider the peaked wave as the sequential limit of smooth wave.
- In the $\log_{10} - \log_{10}$ coordinates of Fourier space, the slope of the linear regression is verified to be approximately -2 for the peaked wave c_* and $-5/3$ for the cusped wave at c_∞ in the linear domain, and large Fourier modes near N persist the non-linearity.

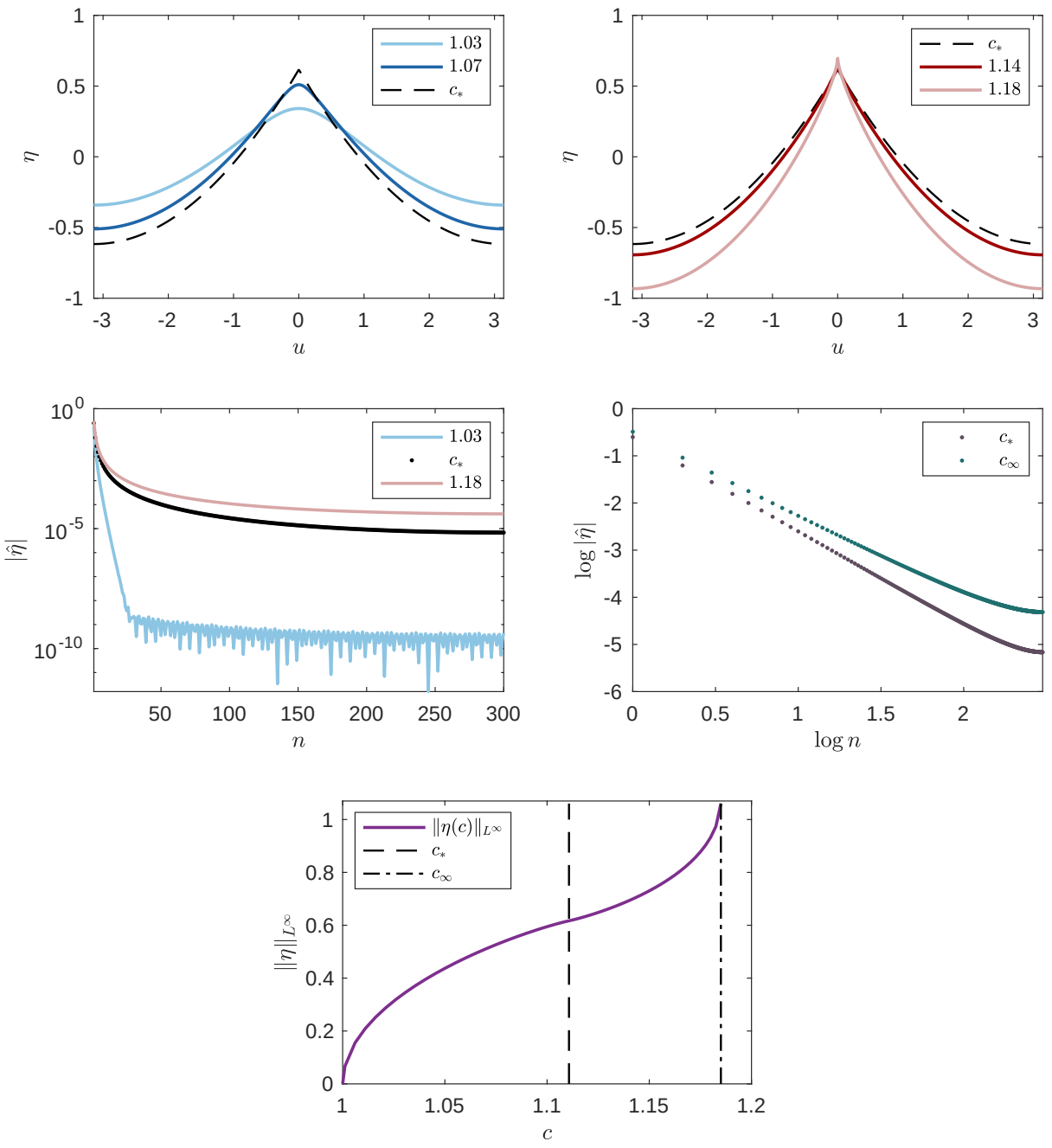

FIGURE 1. (top left & top right) Solution profiles η in physical space for smooth & cusped waves with $N = 300$ grid points and $\epsilon = 10^{-14}$ tolerance for Newton–Raphson's method. The dashed line represent the peaked wave at c_*. (mid left) Solutions in Fourier space $\hat{\eta}$ with $\log_{10} - \log_{10}$ coordinates. (mid right) Solution profiles in Fourier space in logarithmic scale respect to positive Fourier modes $n \in \{0, \ldots, N\}$. (bottom) Sup-norm of solutions respect to $c \in (1, c_\infty)$ with critical values $c_* \approx 1.1107$ and $c_\infty \approx 1.1850$ (dashed lines).

3. Approximation of Eigenvalues

In this section, we implement spectral method on the approximated solution profiles in physical and Fourier space $\eta, \hat{\eta}$ to analyze the spectrum of the local linear operator $\mathcal{L} : H^2_{\text{per}}(\mathbb{T}) \subset L^2(\mathbb{T}) \to L^2(\mathbb{T})$. For sake of notational convenience, we write $\mathcal{L} = \mathcal{M} + \mathcal{W}$ with

$$\mathcal{M} = -\frac{\partial}{\partial u}(c^2 - 2\eta)\frac{\partial}{\partial u}, \qquad \mathcal{W} = (2\eta'' - 1), \tag{14}$$

where $\mathcal{M}$ and $\mathcal{W}$ denotes the kinetic and potential terms. The spectrum of the linearized operator $\mathcal{L}$ can be computed by solving the eigenvalue problem with the 2π-periodic constraint, such that

$$\begin{cases} \mathcal{L}\gamma = \lambda\gamma & u \in \mathbb{T} \\ \gamma(u) = \gamma(u + 2\pi) \end{cases}. \tag{15}$$

Numerically, we apply the finite difference method [12] and the Fourier collocation method [13, 14] to construct the matrix $\mathcal{L}$ in physical and Fourier spaces to solve (15).

3.1. Finite Difference Method.

We first discuss the finite difference method. Based on the approximated of solution profile $\{(u_j, \eta_j)\}_{j=-N}^{N}$ from Section 2 and the central difference approximation of the second derivative $\eta''(u)$, we construct discrete differentiation matrix for local linear operator $\mathcal{L}$ respect to the eigenvector $\gamma = (\gamma_{-N}, \ldots, \gamma_{N-1}) \in \mathbb{R}^{2N}$, such that

$$\mathcal{L} = \begin{bmatrix} (W^0 + \mathcal{M}^0)(\eta_{-N}) & \mathcal{M}^{+1}(\eta_{-N}) & 0 & \cdots & \mathcal{M}^{-1}(\eta_N) \\ \mathcal{M}^{-1}(\eta_{-N+1}) & (\mathcal{W}^0 + \mathcal{M}^0)(\eta_{-N+1}) & \mathcal{M}^{+1}(\eta_{-N+1}) & \cdots & 0 \\ 0 & \mathcal{M}^{-1}(\eta_{-N+2}) & (W^0 + \mathcal{M}^0)(\eta_{-N+2}) & \cdots & 0 \\ \vdots & \vdots & \vdots & \ddots & \vdots \\ \mathcal{M}^{+1}(\eta_{N-1}) & 0 & 0 & \cdots & (\mathcal{W}^0 + \mathcal{M}^0)(\eta_{N-1}) \end{bmatrix}, \tag{16}$$

where the boundary point $\gamma_N(u_N)$ is removed for 2π-periodicity. The diagonal elements $\mathcal{W}^0(\eta_j)$ and off-diagonal elements $\mathcal{M}^{\pm 1}(\eta_j)$ for $j \in \{-N, \ldots, N-1\}$ can be written as

$$\begin{cases} \mathcal{M}^0(\eta_j) = \frac{2c^2 - 2\eta_j - \eta_{j+1} - \eta_{j-1}}{h^2} \\ \mathcal{M}^{\pm 1}(\eta_j) = -\frac{c^2 - \eta_j - \eta_{j\pm 1}}{h^2} \end{cases}, \ \mathcal{W}^0(\eta_j) = \begin{cases} \frac{4\mathcal{E} + 2\eta_j^2 - 2c^2\eta_j}{(c^2 - 2\eta_j)^2} - 1 & c \in (1, c_*) \\ -\frac{1}{2} - \pi\delta(u_j) & c = c_* \end{cases}, \ \delta(u_j) \approx \frac{1}{\sqrt{\pi\alpha^2}} e^{-u_j^2/\alpha^2}. \tag{17}$$

In this construction, we included the eigenfunctions of both even and odd parities. For the kinetic term, since we only consider linear stability, each midpoint of two adjacent grid points is approximated by linear interpolation. In the potential term, the second derivatives are computed from the first derivatives based on the ODE (2) for the smooth waves $c \in (1, c_*)$. The peaked wave at $c = c_*$ has the second derivative $\eta'' = 1/4$ for $u \in \mathbb{T}\backslash\{0\}$, and the singularity at $u = 0$ is accommodated by the Dirac-δ function, which is further approximated by the Gaussian function with a small $\alpha > 0$ in equation (17).

By diagonalization of matrix (16), the first five eigenfunctions γ are plotted in Figure 2, and the first five eigenvalues are plotted in Figure 4.

Remark 3. The Figure 2 shows the eigenfunctions corresponding to $\lambda_1, \ldots, \lambda_5$ for smooth waves with $c \in (1, c_*)$, and we address some important patterns below.

- The first eigenfunction γ_1 approaches Dirac-δ in the limit, but since it is numerically approximated by Gaussian function, there is a slight broadening. This also explains the reason for $\lambda_1 \to -\infty$ as $c \to c_*^-$ in Figure 4.
- Without the consideration of λ_1, the eigenfunctions corresponding to even eigenvalues $\lambda_{2l}, l \in \mathbb{Z}^+$ are in even parity, and the eigenfunctions corresponding to the odd eigenvalues $\lambda_{2l+1}, l \in \mathbb{Z}^+$ are in odd parity.
- The inaccurate eigenvalues is because of the poor convergence of solutions profiles in Fourier space, see Remark 2.

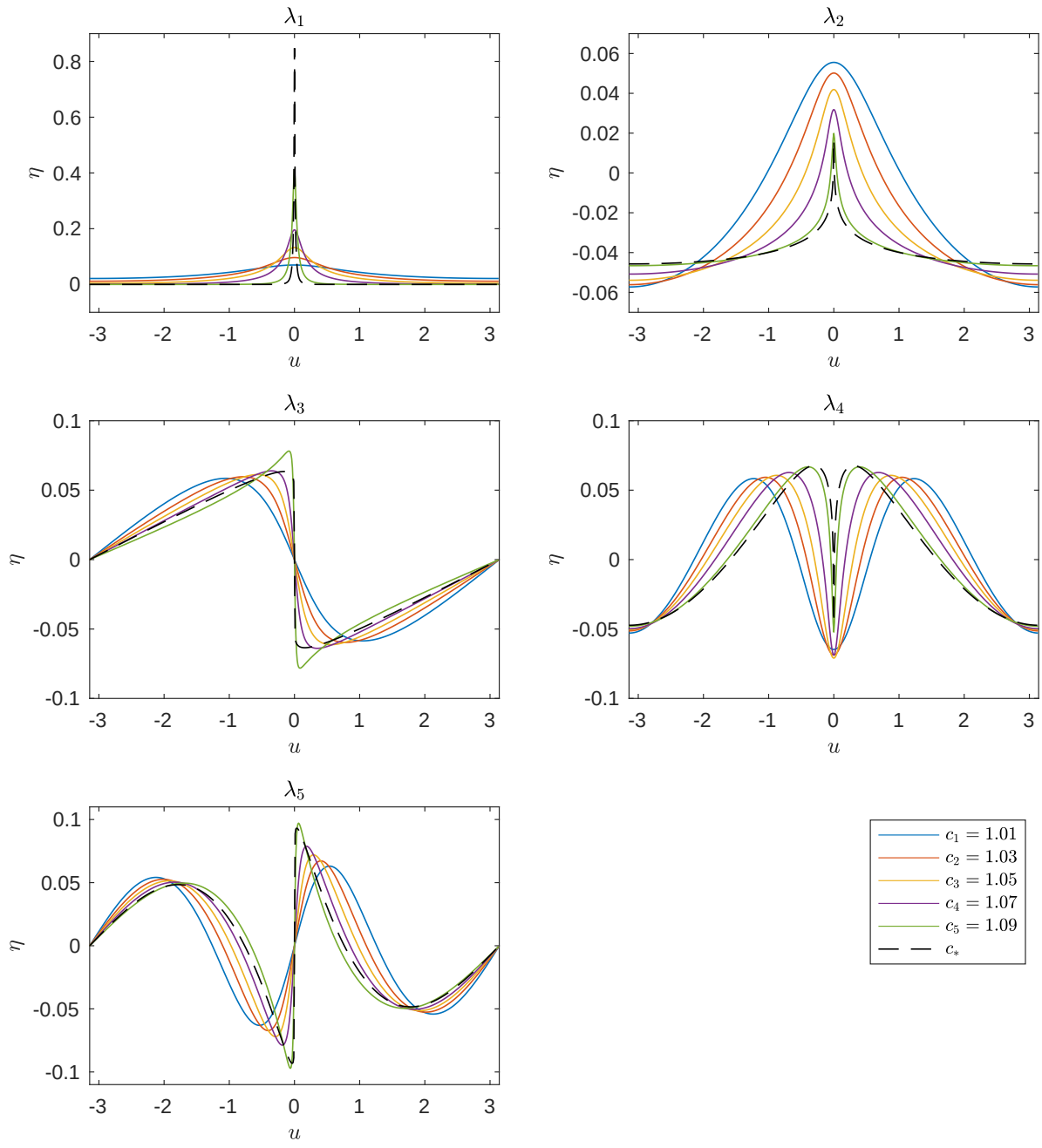

FIGURE 2. The smooth (solid) and peaked (dashed) wave eigenfunctions corresponding to the first five eigenvalues for $c \in (1, c_*]$. The grid in physical space is chosen to be $N = 300$, and the Gaussian parameter takes the step size $\alpha = \pi/N$. The solution profiles obtained from equation (11) are used for diagonalization, and all eigenfunctions are plotted on $[-\pi, \pi]$ with positive slope near $-\pi$.

3.2. **Fourier Collocation Method.** In this part, we discuss the Fourier collocation method. By analogy to the solutions in Fourier space $\hat{\eta}$ from (11), we write its perturbation $\hat{\gamma} = (\hat{\gamma}_{-N}, \dots, \hat{\gamma}_N) \in \mathbb{R}^{2N+1}$ by DFT, such that

$$\hat{\gamma}_m = \frac{h}{2\pi} \sum_{j=-N}^{N-1} \gamma_j e^{-imu_j}, \qquad m \in \{-N, \dots, N\} \tag{18}$$

Since the L^2-isomorphism between physical and Fourier space, we solve the eigenvalue problem in Fourier space $\widehat{\mathcal{L}}\hat{\gamma} = \lambda\hat{\gamma}$ where $\widehat{\mathcal{L}} = \widehat{\mathcal{M}} + \widehat{\mathcal{W}}$ is the local linear operator in Fourier space, such that

$$\widehat{\mathcal{M}} = 2(\mathcal{D}_1\hat{\eta})\mathcal{D}_1 - c^2\mathcal{D}_2 + 2\hat{\eta}\mathcal{D}_2, \qquad \widehat{\mathcal{W}} = \begin{cases} 2(D_2\hat{\eta}) - \pi I & c \in (1, c_*) \\ -\frac{1}{2}I - \mathbb{I} & c = c_* \end{cases}. \tag{19}$$

where the first and second derivative are diagonal and determined as

$$\mathcal{D}_1 = i\,\mathrm{diag}(-N, \dots, N), \qquad \mathcal{D}_2 = \mathcal{D}_1^2. \tag{20}$$

Equation (19) can be considered as the Fourier transform of equation (17), and the solution profiles in Fourier space $\hat{\eta}$ are constructed by matching up the Fourier modes for $m \in \{-N, \dots, N\}$, and the unity $\mathbb{I}$ can be constructed in the similar manner as Toeplitz matrices, such that

$$\hat{\eta} = \begin{bmatrix} \hat{\eta}_0 & \cdots & \hat{\eta}_{-N} & \cdots & 0 \\ \vdots & \ddots & \vdots & \ddots & \vdots \\ \hat{\eta}_N & \cdots & \hat{\eta}_0 & \cdots & \hat{\eta}_{-N} \\ \vdots & \ddots & \vdots & \ddots & \vdots \\ 0 & \cdots & \hat{\eta}_N & \cdots & \hat{\eta}_0 \end{bmatrix}. \qquad \mathbb{I} = \begin{bmatrix} 1 & \cdots & 1 & \cdots & 0 \\ \vdots & \ddots & \vdots & \ddots & \vdots \\ 1 & \cdots & 1 & \cdots & 1 \\ \vdots & \ddots & \vdots & \ddots & \vdots \\ 0 & \cdots & 1 & \cdots & 1 \end{bmatrix}. \tag{21}$$

By solving the eigenvalue problem in Fourier space, Figure 3 plots the eigenfunctions of first five eigenvalues with logarithmic scale in $|\hat{\gamma}|$.

Remark 4. The Figure 3 shows the eigenfunctions corresponding to first five eigenvalues in the Fourier space for the smooth waves, and we make some remarks below. .

- The eigenfunctions do not converge well to zero when $c \to c_*^-$, see, e.g., graphs for $c = 1.09$. This indicates the loss of accuracy.
- Depending on the number of grid point N, the convergence behaviour varies. The eigenfunctions decay well for a given value of c with more grid, but if $c \to c_*^-$ for a fixed grid, the decay of eigenfunctions is broken.

Here, we also remark the results of eigenvalue obtained from both 3.1 and 3.2. The eigenvalues and relevant properties are shown and compared in Figure 4.

Remark 5. The Figure 4 shows the first five eigenvalues for smooth waves $c \in (1, c_*)$, and we extends the case to the peaked wave $c = c_*$. The number of grid points N is also taken into consideration.

- The first eigenvalue λ_1 diverges to $-\infty$ as $c \to c_*^-$.
- The third eigenvalue λ_3 is identically zero for some $\tilde{c} < c_*$, and it deviates from zero before the limit of peaked wave. This does not agree with theorem 2 since the zero eigenvalue ($\lambda_3 = 0$) is expected to persist for all $c \in (1, c_*)$.
- The deviation of λ_3 in the limit $c \to c_*$ indicates the loss of numerical accuracy, so the spectrum obtained for the singular peaked wave is invalid.
- This deviation happens in both the finite difference and Fourier collocation methods.
- With the increase of grid point, the deviation point $\tilde{c}$ approaches c_*, but the loss of accuracy cannot be avoided fundamentally.

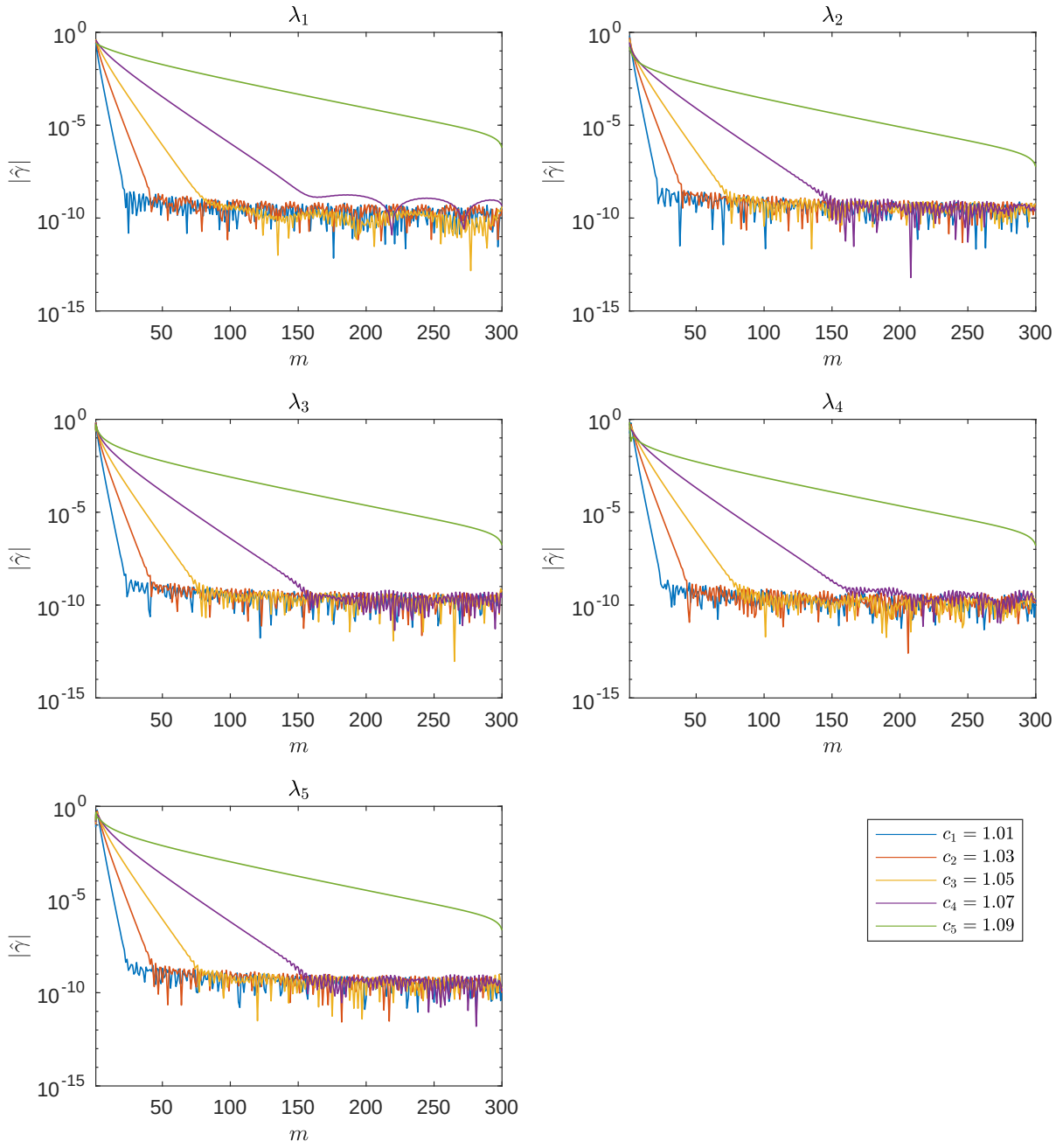

FIGURE 3. The absolute value of smooth wave eigenfunctions $|\hat{\gamma}|$ in Fourier space corresponding to first five eigenvalues are plotted respect to the half of Fourier modes $m \in \{1, \ldots, N\}$ for $c \in (1, c_*)$. The grid in physical space is chosen to be $N = 300$, and the solution profiles $\hat{\eta}$ are obtained from equation (11) and (12).

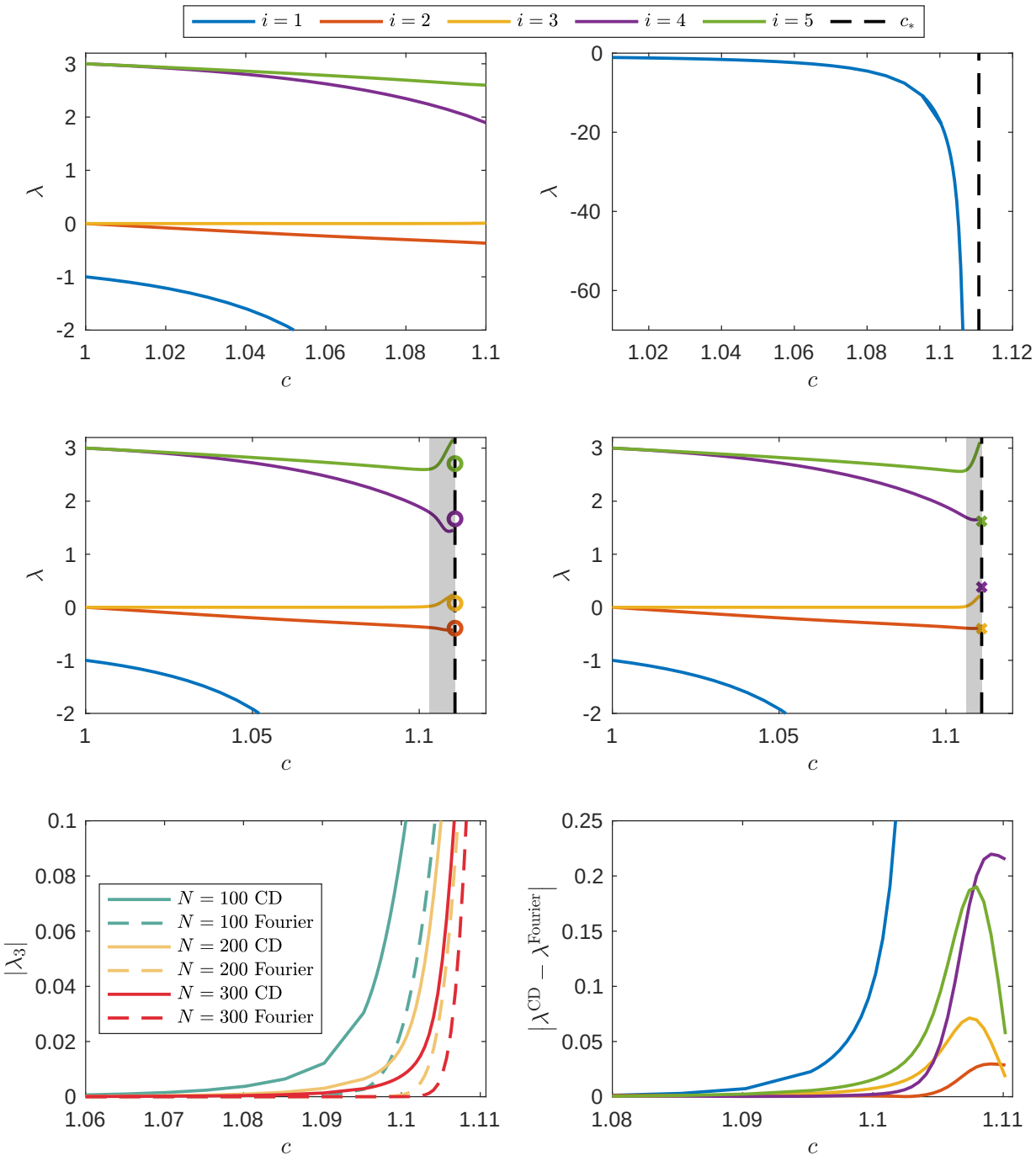

FIGURE 4. (top left & right) The spectrum of first five eigenvalues $\lambda_i, i = 1, \ldots, 5$ in $c \in (1, c_*]$ is plotted. The first eigenvalue diverges to $-\infty$, and the loss of numerical accuracy happens when $c \to c_*^-$ (shaded). (middle left & right) First five eigenvalues are obtained by the finite difference & Fourier collocation method, and values at c_* are marked as circles & stars. (bottom left) The third eigenvalue $|\lambda_3|$ deviates from 0 as $c \to c_*^-$ for different grids $N = 100, 200, 300$ by the finite difference (CD) and Fourier collocations methods. (bottom right) Errors between each eigenvalues are shown for both methods.

References

[1] G. G. Stokes, "On the Theory of Oscillatory Waves", Transactions of the Cambridge Philosophical Society **8** (1847) 441-455.

[2] S. Locke and D. E. Pelinovsky, "On smooth and peaked traveling waves in a local model for shallow water waves", math.AP **arXiv:2406.06722** (2024).

[3] W. M. Drennan, W. H. Hui and G. Tenti, "Accurate calculations of Stokes water waves of large amplitude", Zeitschrift für Angewandte Mathematik und Physik **43** (1992) 367–384.

[4] C. J. Amick, L. E. Fraenkel, J. F. Toland, "On the Stokes conjecture for the wave of extreme form", Acta Mathematica **148** (1982) 193-214.

[5] W. Craig, D. P. Nicholls, "Traveling gravity water waves in two and three dimensions", European Journal of Mechanics B **21** (2002) 615-641.

[6] G. G. Stokes, "Supplement to a paper on the theory of oscillatory waves", Mathematical and Physical Papers **1** (1880) 314–326.

[7] V. E. Zakharov, "Stability of periodic waves of finite amplitude on a surface", Journal of Applied Mechanics and Technical Physics **9** (1968) 190–194.

[8] J. K. Hunter, R. Saxton, "Dynamics of director fields", SIAM Journal on Applied Mathematics **51** (1991) 1498-1521.

[9] R. Camassa, D. D. Holm, " An integrable shallow water equation with peaked solitons", Physics Review Letter **71** (1993) 1661–1664.

[10] J. K. Hunter, Y. Zheng, "On a completely integrable nonlinear hyperbolic variational equation", Physics D **79** (1994) 361-386.

[11] A. Madiyeva, D. E. Pelinovsky, "Growth of perturbations to the peaked periodic waves in the Camassa-Holm equation", SIAM Journal on Mathematical Analysis **53** (2021) 3016–3039.

[12] M. Grasselli, D. E. Pelinovsky, *Numerical Mathematics* (Jones & Bartlett Learning, 2007).

[13] L. N. Trefethen, *Spectral Methods in MATLAB* (SIAM, 2000).

[14] J. Yang, *Nonlinear Waves in Integrable and Non-integrable Systems*, (SIAM, 2010).

Email address: wangs455@mcmaster.ca, dmpeli@math.mcmaster.ca